JHEP PROCEEDINGS

Heavy Flavours 8, Southampton, UK, 1999

Status of the BABAR Experiment

Roland Waldi

*Inst. f. Kern- und Teilchenphysik**
Technische Universität Dresden, 01062 Dresden, Germany
for the BABAR Collaboration
Email: waldi@physik.tu-dresden.de

ABSTRACT: The *BABAR* detector at the B Meson Factory PEP II (SLAC) has started data taking this year. First performance figures will be presented.

1. Introduction

Since the discovery of CP violation in neutral kaon decays in 1964 [1], the understanding of this then tiny effect has made big progress. The Standard Model (SM) with three families of quarks can explain CP violation as an interference due to the physical phase in the unitary Cabibbo-Kobayashi-Maskawa (CKM) mixing matrix [2]. Large asymmetries in the time dependent decay rates $\dot{N}$ of neutral B mesons are predicted in this model [3], which can be parametrized as

$$a(\Delta t) = \left.\frac{\dot{N}(B^0+X)-\dot{N}(\overline{B}^0+X)}{\dot{N}(B^0+X)+\dot{N}(\overline{B}^0+X)}\right|_{\Delta t} = \Theta_0 \cos x\frac{\Delta t}{\tau} + \Lambda_0 \sin x\frac{\Delta t}{\tau} \qquad (1.1)$$

where Δt is the difference of the lifetimes of the two B mesons from an $\Upsilon(4S)$ decay, if one reveals its flavour as B^0 or $\overline{B}^0$ and the second decays into a final state X that can be reached from both. The parameters Θ_0 and Λ_0 can be measured from a fit to this time-dependent asymmetry, and are related to the phase angles in the CKM unitarity triangle, e.g. for CP eigenstates $c\bar{c}d\bar{d}$, $c\bar{c}K^0_S$ or $c\bar{c}K^0_L$, $\Theta_0 = 0$ and $\Lambda_0 = \sin 2\beta$.

2. PEP II

These measurements will be pursued at various B meson factories. One of them is PEP II, which was approved in 1993, and has started operation with the *BABAR* detector in place in May 1999. It is an asymmetric e^+e^- collider, with a low energy positron beam of 3.1 GeV and a high energy electron beam of 9 GeV. Thus, $B\overline{B}$ pairs are produced from $\Upsilon(4S)$ decays with a boost of $\beta\gamma = 0.56$ in the beam direction, and their lifetime difference can be measured via the distance in their vertex positions along the beam axis Δz.

At startup, PEP II was operated at one quarter of the design number of bunches. The machine has delivered an initial luminosity of $0.2 \cdot 10^{33}/\mathrm{cm}^2/\mathrm{s}$, which was gradually raised to $1.4 \cdot 10^{33}/\mathrm{cm}^2/\mathrm{s}$ in September. This was achieved mainly by increasing the number of particles per bunch and by improvements in the interaction point focus. We expect to reach the design luminosity of $3 \cdot 10^{33}/\mathrm{cm}^2/\mathrm{s}$ in the year 2000, and see a potential for a further increase in the coming years. The integrated luminosity taken by *BABAR* at the time of the conference was about 100/pb, and by now more than 1/fb have been accumulated.

3. The BABAR Detector

Figure 1 shows a schematic view of the *BABAR* detector components, in a cut along the beam axis.

The first months of detector operation were characterized by work on calibration and performance optimization, and lead to steady improve-

*supported by Bundesministerium für Bildung, Wissenschaft, Forschung und Technologie, Germany, under contract 06DD558I.

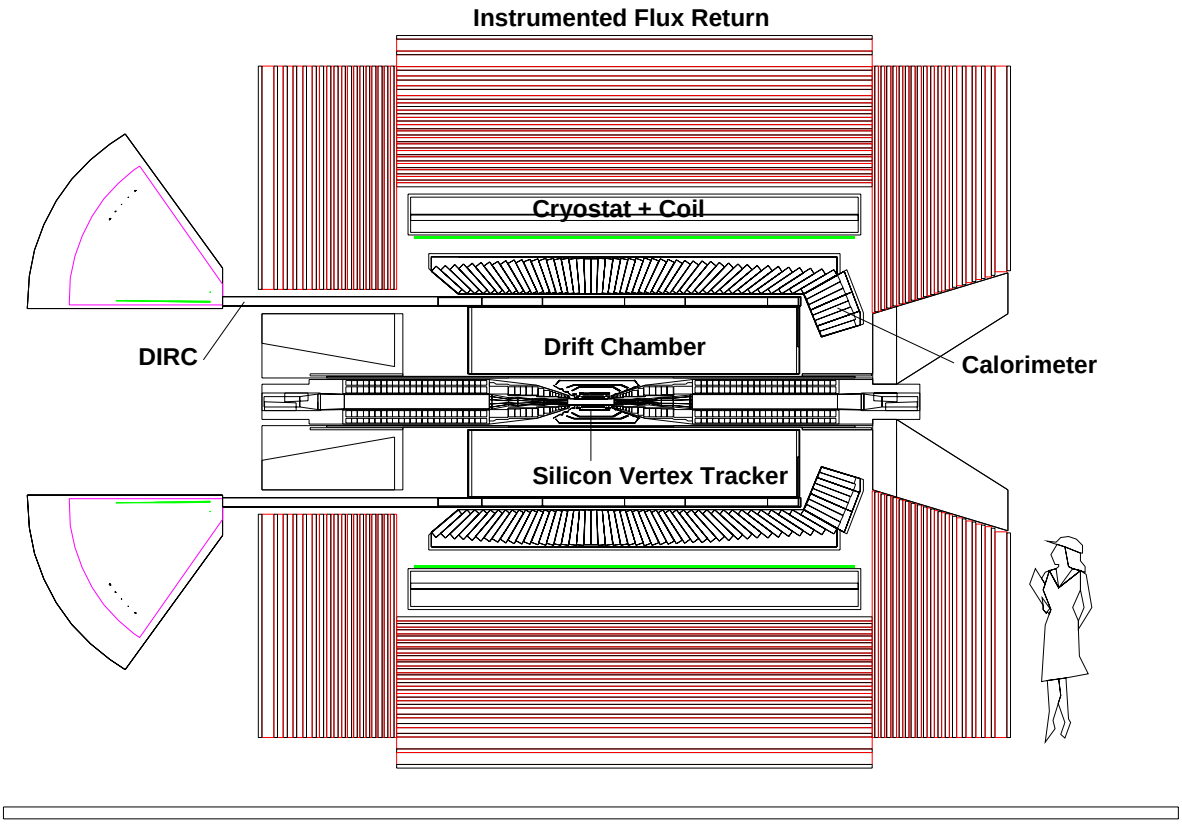

Figure 1: Schematic view of the *BABAR* detector cut along the beam axis. The focusing quadrupoles and the beam separation dipoles are inside the detector, leaving only limited space for the silicon vertex detector. Both are surrounded by a cylindrical drift chamber, followed in radial direction by the DIRC, the Cs I calorimeter, the superconducting magnet coil and the instrumented flux return (IFR).

ments. A snapshot of performance figures will be given in the next sections.

The vertex detector information dominates the measurement of the track impact parameters, both along and perpendicular to the beam direction. The *BABAR* silicon vertex tracker (SVT) consists of five layers of two-sided 300 μm thick silicon strip detectors. The innermost three are arranged as hexagonal prisms around the beam axis, with a pitch of 50 and 100 μm. The outer two are arranged in shapes close to cylinders or cones centred at the beam axis, and use pitch values between 65 and 210 μm. The angular acceptance for the entire experiment is determined by the vertex detector, which is limited by machine components, and extends from $-0.87 < \cos\theta_{\rm lab} < 0.96$, which transforms into $-0.95 < \cos\theta_{\rm cms} < 0.87$ in the e^+e^- centre of mass system. Tracks with transverse momentum between 40 MeV/c and about 100 MeV/c are reconstructed primarily in the silicon tracker.

Proper alignment data for all wafers as well as the relative alignment between SVT and drift chamber are the crucial inputs to achieve the required vertex resolution. The spatial resolution achieved so far in the innermost layer, as determined from our first months of data, is shown in figure 2, and is already close to our expectations from the Monte Carlo simulation.

The direction of charged tracks is determined primarily in the vertex detector, while the curvature is measured in the drift chamber. It has 7104 hexagonal drift cells with signal wires either parallel to the detector axis or at stereo angles between 42 and 70 mrad. Its angular

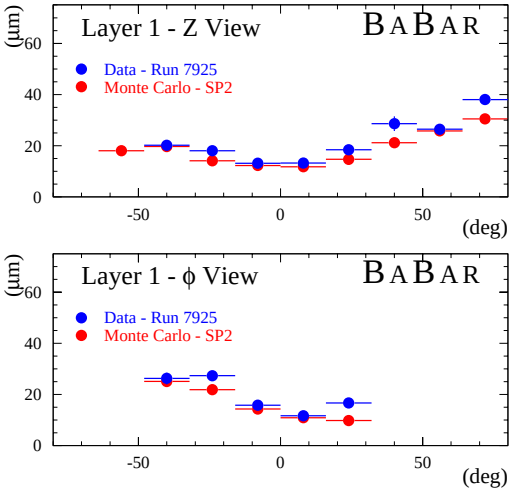

Figure 2: Measured spatial resolution in the first SVT layer as a function of the impact angle, compared to Monte Carlo expectation.

acceptance matches that of the vertex detector.

The superconducting magnet coil provides a field of 1.5T inside the tracking volume. Together with the spatial resolution, which is shown in figure 3 for our present data, this allows a momentum accuracy close to our design value of 0.3% for high-momentum tracks.

The full tracking system, consisting of SVT and drift chamber, provides very good pattern recognition capability for charged tracks even at occasional periods with high machine background. Already in the very first data, a sample of less than 3/pb integrated luminosity, a clear peak in the mass difference of $K^-\pi^+\pi^+$ and $K^-\pi^+$ combinations from the $D^{*+} \to D^0\pi^+$ decay is visible (see figure 4), which comprises low-momentum pions reconstructed in the SVT as well as pions from drift chamber tracks.

The pulse height information from drift chamber signals is used to measure the mean ionization loss (dE/dx). The present calibration gives typical resolutions of the truncated mean of 8%; for Bhabha electrons 7% resolution has been reached, which is about the limit expected with a helium and isobutane gas mixture.

There are two important benchmarks of performance for the particle identification system. One is the ability to separate $B^0 \to \pi^+\pi^-$ from $B^0 \to K^+\pi^-$ and the other is the performance of charged kaon tagging. In the barrel region, these requirements are met by a DIRC (**d**etection of **i**nternally **r**eflected **C**herenkov light), a special sort of ring-imaging Cherenkov detector.

The DIRC radiator consists of 156 quartz bars of 4.7m length arranged in a 12-sided polygon around the drift chamber. A charged particle traversing a bar produces Cherenkov light which is emitted at the Cherenkov angle with respect to the particle direction. Part of this light hits the bar walls beyond the angle of total reflection, and is multiply reflected, until it reaches the back end, where it is transmitted via the standoff box—a water-filled tank—to an array of photomultiplier tubes. The directions of the reflected part of the Cherenkov cone form two conic sections in the detector plane, which define the Cherenkov angle and thereby the velocity of the charged particle.

When *BABAR* started data taking in May, five of these boxes were filled with quartz bars, and were used to study the performance in first data. In a recent shutdown in mid-October, the remaining bars were inserted, and *BABAR* is now operating with the DIRC covering the full azimuthal angle.

Achieving the desired sensitivity for measuring asymmetries in CP decay modes such as $J/\psi K^0_S$, $J/\psi K^{*0}$, $D^{*+}D^{*-}$, and $\rho^\pm\pi^\mp$ requires observing π^0 mesons with very high efficiency and good resolution. This is the physics goal

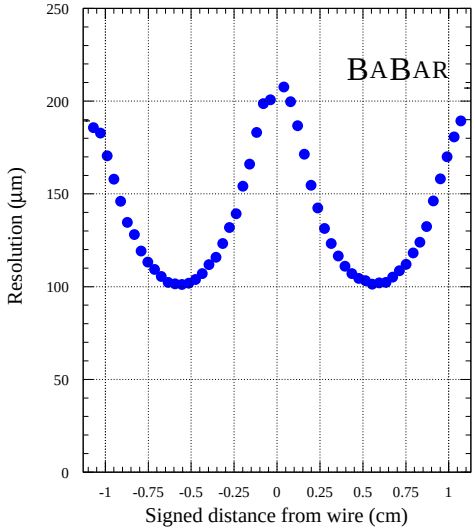

Figure 3: Measured spatial resolution in the drift chamber as a function of the distance from the signal wire.

which drives the performance requirements of the electromagnetic calorimeter.

The photon energy region of interest for B physics ranges from about 20 MeV to 4 GeV in the laboratory. The B mass resolution for modes such as $\pi^0\pi^0$ or $\rho\pi$ is dominated by the photon energy resolution. The optimum calorimeter design to achieve good resolution over this wide range is a structure of Tl-doped Cs I crystals. They are arranged in a barrel and a forward endcap, with their axes pointing close to the interaction region. They are inside the magnet coil, and are read out by two silicon photodiodes each.

The energy resolution at normal incidence achieved with a prototype is about 2.1% at 200 MeV (FWHM/2.36), and a detailed Monte Carlo simulation predicts about 1.6% at 1 GeV. While the calibration of the real calorimeter is not yet final, we already see a reasonably narrow π^0 signal. Figure 5 shows the invariant mass of all combinations of neutral clusters (photon candidates) above 100 MeV with an energy sum above 500 MeV. The π^0 peak is found at a value below its true mass, since cluster energies are not yet corrected for leakage. The width of 8.5MeV is still above the expectation from our Monte Carlo simulation, due to the incomplete calibration.

The barrel calorimeter covers the range $-0.78 < \cos\theta_{\rm lab} < 0.89$; the forward endcap calorimeter extends the forward coverage to $\cos\theta_{\rm lab} < 0.95$. In the centre of mass the full acceptance of a shower

is in the range $-0.91 < \cos\theta_{\rm cms} < 0.87$.

The primary goal of the instrumented flux return (IFR) is to reduce the lower momentum limit for cleanly identifying muons to about $0.6\,{\rm GeV}/\cos\theta_{\rm lab}$. This increases the efficiency for tagging the flavour of a B meson substantially, and it also increases the size of the lepton sample for studies of semileptonic decays. The thickness of the iron layers is graded from 2 cm on the inside to 5 cm on the outside. The finer segmentation of the innermost layers is chosen to identify muons of the lowest possible momentum. The gaps are filled with resistive plate chambers, which offer a reliable and relatively cheap solution for the 2500 $\rm m^2$ of active area to be covered. In addition to its primary goal to identify muons, the IFR can identify K^0_L mesons to measure their angle reasonably well to detect $B^0 \to J/\psi\, K^0_L$.

4. The $\Upsilon(4S)$ Resonance Scan

From June 14 to 17, 1999, we had a first scan over the $\Upsilon(4S)$ resonance region. One third of the data at each energy point was reconstructed immediately, and is the basis of a preliminary analysis.

Figure 4: Mass difference of $K^-\pi^+\pi^+$ and $K^-\pi^+$ combinations from the very first data. A pronounced peak from $D^{*+} \to D^0\pi^+$ is observed.

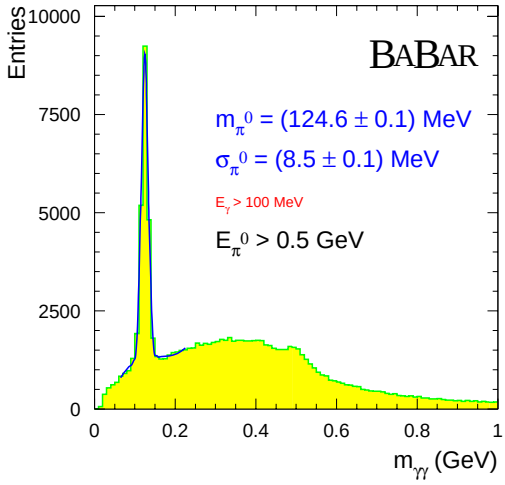

Figure 5: Combining two neutral calorimeter clusters reveals a clear π^0 peak.

For the cross section determination, two event classes have been selected: multihadron final states with at least four charged tracks, and Bhabha events with two tracks back-to-back in the e^+e^- centre of mass. The cross section for the latter is precisely known and scales within the scan interval with $1/s$, so their number gives an accurate measure of the relative luminosities per data sample. The angular distribution of electrons and positrons from these events is compared to the QED prediction in figure 6. The agreement demonstrates that this class of events has a uniform acceptance over the chosen fiducial volume, and gives a reliable measurement of integrated luminosity.

The fraction of $\Upsilon(4S)$ events in the multihadron sample can be adjusted within a wide range by a cut on the normalized second Fox–Wolfram moment H_2 evaluated in the cms, which varies from 0 for isotropic events to 1 for extreme back-to-back jets. The ratio of the number of multihadron events to the number of Bhabha events (scaled to one energy with the $1/s$ law) is submitted to a fit of the cross section function

$$\sigma(E) = \frac{P_0}{s} + R(s|\Gamma, M, B_{ee}, \Delta)$$

with the argument E = nominal PEP II cms energy. This is converted via $\sqrt{s} = E - M +$

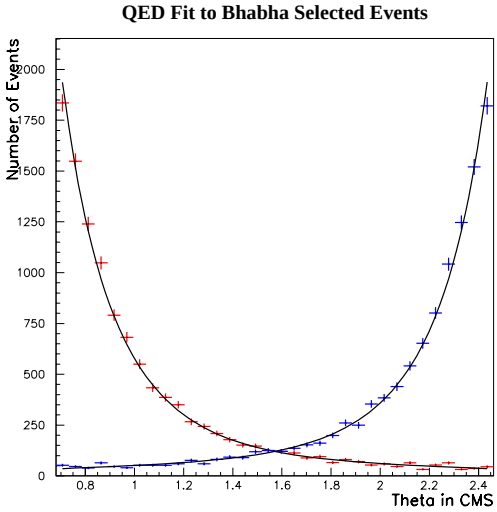

Figure 6: Polar angle distribution of electrons and positrons from Bhabha scattering in the centre of mass system, compared to the QED expectations.

$M_{\Upsilon(4S)}$ into a cms energy relative to the world average mass [4] of the $\Upsilon(4S)$ which is strongly coupled to the measurement of B meson masses. This conversion insures that the resonance shape is independent of a potential PEP II energy scale bias.

The resonance function $R(s|\Gamma, M, B_{ee}, \Delta)$ is determined by the physical Breit Wigner shape

$$\sigma_0(s) = 12\pi \frac{\Gamma_{ee}(s)\,\Gamma(s)}{(s-M^2)^2 + M^2\Gamma^2(s)}$$

where the quark pair creation model [5] has been used to parametrize $\Gamma(s)$. This approach includes the rapid variation of the $B\overline{B}$ two body phase space as well as corrections from the wave function overlap of $\Upsilon(4S)$ and B mesons. This cross section is modified by radiative corrections, including events of the type $e^+e^- \rightarrow \gamma\Upsilon(4S)$, and by the beam energy spread in the storage ring due to synchrotron radiation, which is parametrized as a Gaussian distribution with standard deviation Δ.

Free fit parameters are the continuum normalization P_0, the $\Upsilon(4S)$ mass M on the nominal PEP II cms energy scale, the physical resonance width $\Gamma = \Gamma(M_{\Upsilon(4S)})$, and the e^+e^- branching fraction at the physical mass $B_{ee} = \Gamma_{ee}/\Gamma$. The cms energy spread from synchrotron radiation, Δ, is taken as a constant, with its best estimated value of $\Delta = 5.30\,\mathrm{MeV}$.

A first look at the data is seen in figure 7. The peak mass on the uncalibrated PEP II energy scale turned out to be within 5MeV of the known mass of (10580.0 ± 3.5)MeV [4]. This demonstrates a precision of the PEP II orbit calculations of $5 \cdot 10^{-4}$ or better. The width of 12 ± 5MeV is compatible with the ARGUS measurement [6], and will be determined with an accuracy better than $\pm$1MeV from the full data sample and some high-statistics runs on and off resonance. The determination of B_{ee} requires proper normalization of the cross section, including detailed acceptance studies for $B\overline{B}$ and Bhabha events. These investigations are in progress.

5. Outlook

In addition to this analysis, which will be finished in a few months, *BABAR* will pursue a broad agenda of physics involving the heavy quark and heavy lepton sector. The focus of our interest is the measurement of CP violation parameters in the B meson system. We expect to have collected a sample of 10/fb on the $\Upsilon(4S)$ by summer 2000, which will allow us to present first results on $\sin 2\beta$ around this time.

References

[1] J.H.Christenson, J.W. Cronin, V.L. Fitch, R. Turlay, *Phys. Rev. Lett.* **13** (1964) 138.

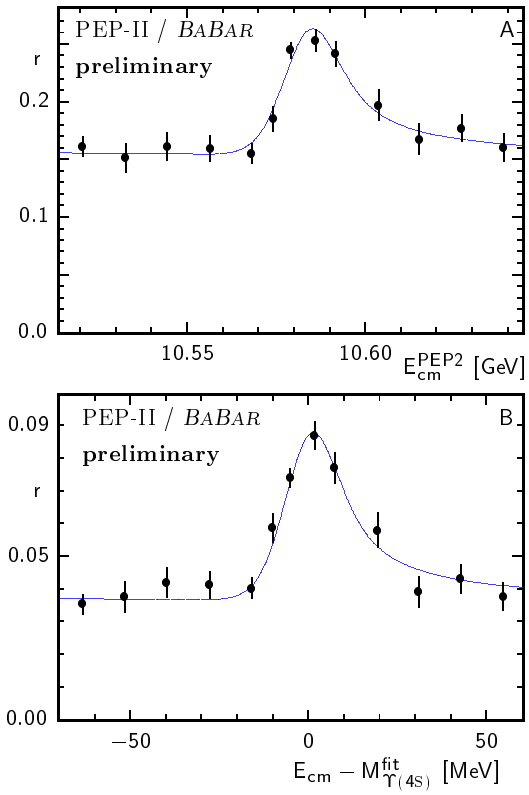

Figure 7: The preliminary analysis of 3/pb of the Υ(4S) scan shows the ratio of multihadron events selected with $H_2 < 0.5$ (A) and $H_2 < 0.2$ (B) and the number of Bhabha events scaled with s. The peak position is used to set the PEP II energy scale, requiring the fitted mass to be 10.580 GeV. It is determined with a precision of ± 0.7 MeV. The total width is 12 ± 5 MeV.

[2] M.Kobayashi, T.Maskawa, *Prog. Theor. Phys.* **49** (1973) 652.

[3] I.I.Bigi, A.I.Sanda, *Nucl. Phys.* **B 193** (1981) 85.

[4] The Particle Data Group, C.Caso *et al.*, *Eur. Phys. J.* **C 3** (1998) 1.

[5] A. Le Yaouanc, L.Oliver, O.Pene, C.Raynal, *Phys. Rev.* **D 8** (1973) 2223; A. Le Yaouanc *et al.*, *Phys. Lett.* **B 71** (1977) 397; S.Ono, *Phys. Rev.* **D 23** (1981) 1118.

[6] ARGUS Collab., H.Albrecht *et al.*, *Z. Physik* **C 65** (1995) 619.